Multifunctional Role of Rare Earth Doping in Optical Materials: Nonaqueous Sol–Gel Synthesis of Stabilized Cubic HfO_2 Luminescent Nanoparticles

Alessandro Lauria,[†,*] Irene Villa,[‡] Mauro Fasoli,[‡] Markus Niederberger,[†] and Anna Vedda[‡]

[†]Laboratory for Multifunctional Materials, Department of Materials, ETH Zurich, Wolfgang-Pauli-Strasse 10, 8093 Zurich, Switzerland, and [‡]Department of Materials Science, University of Milano–Bicocca, Via R. Cozzi 53, 20125 Milano, Italy

ABSTRACT In this work a strategy for the control of structure and optical properties of inorganic luminescent oxide-based nanoparticles is presented. The nonaqueous sol–gel route is found to be suitable for the synthesis of hafnia nanoparticles and their doping with rare earths (RE) ions, which gives rise to their luminescence either under UV and X-ray irradiation. Moreover, we have revealed the capability of the technique to achieve the low-temperature stabilization of the cubic phase through the effective incorporation of trivalent RE ions into the crystal lattice. Particular attention has been paid to doping with europium, causing a red luminescence, and with lutetium. Structure and morphology characterization by XRD, TEM/SEM, elemental analysis, and Raman/IR vibrational spectroscopies have confirmed the occurrence of the HfO_2 cubic polymorph for dopant concentrations exceeding a threshold value of nominal 5 mol %, for either Lu^{3+} or Eu^{3+}. The optical properties of the nanopowders were investigated by room temperature radio- and photoluminescence experiments. Specific features of Eu^{3+} luminescence sensitive to the local crystal field were employed for probing the lattice modifications at the atomic scale. Moreover, we detected an intrinsic blue emission, allowing for a luminescence color switch depending on excitation wavelength in the UV region. We also demonstrate the possibility of changing the emission spectrum by multiple RE doping in minor concentration, while deputing the cubic phase stabilization to a larger concentration of optically inactive Lu^{3+} ions. The peculiar properties arising from the solvothermal nonaqueous synthesis here used are described through the comparison with thermally treated powders.

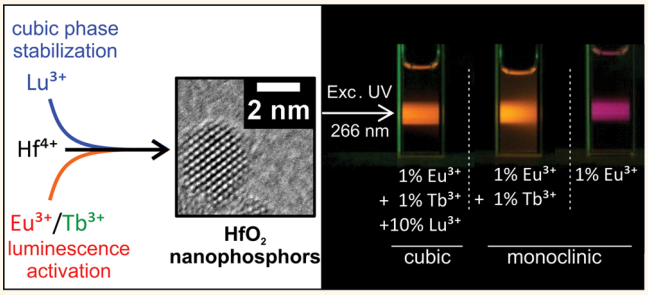

KEYWORDS: hafnia · cubic lattice · lutetium · europium · luminescence · nonaqueous sol–gel · nanoparticle · rare earth

Hafnium dioxide, or hafnia, possesses several outstanding chemical and physical properties making it attractive for a variety of applications. It has been studied over the last decades, mainly in the form of thin films, due to its higher dielectric constant (ε = 25) with respect to silica, a property suitable for its application as new generation high-k gate dielectric in microelectronics.[1,2] As a result of its very high melting point (over 2700 °C) and its mechanical resistance,[3,4] hafnia has also found application in refractory protective coatings of thermocouples in harsh conditions as in nuclear applications.[5] More recently, hafnia has been considered because of its transparency in the visible range (band gap = 5.3–5.9 eV).[6] Together with chemical inertness, this makes HfO_2 an interesting material for optical applications, when acting as host for rare earths (RE) ions meant as luminescent activators.[7–11]

Nevertheless, a complete and extensive characterization of the optical properties of HfO_2 is still not reported in the literature, especially due to its high melting point which makes the preparation of the material as a bulk still a major issue. The development of effective and facile wet chemical syntheses has played a key role in increasing the knowledge on its potential for novel

* Address correspondence to alessandro.lauria@mat.ethz.ch.

Received for review May 10, 2013 and accepted July 30, 2013.

Published online July 30, 2013
10.1021/nn402357s

applications.[12] Monoclinic HfO_2 doped with several rare earth ions has been prepared by hydrothermal and Pechini-based sol–gel method and its optical emission has been reported.[13,14] In addition, the non-hydrolithic sol–gel method (NHSG) has already been demonstrated to be a suitable way for the synthesis of HfO_2 nanoparticles (NPs) with a diameter well below 5 nm.[15,16] Through the appropriate choice of precursors, the effective incorporation of doping elements can also be easily achieved by this technique involving a mechanism in which the crystal growth is operated at relatively low temperatures. The contemporary solvolysis reaction with benzyl alcohol of both host and dopants precursors leads to the formation of the oxide.[17]

Since all wet methods lead to the production of crystalline powders that are intrinsically affected by light scattering, a further processing is required in order to obtain transparent materials suitable for optical applications. Aiming at future exploitation, a couple of possible strategies could be adopted. (i) On one hand, the embedding of particles into a transparent host can be pursued: in this case, downscaling of luminescent particles down to the nanometric size is desirable for scattering minimization. (ii) On the other hand, the fabrication of optical ceramics by powder-sintering can be performed, where the cubic symmetry is necessary due to its isotropic optical properties, so to avoid scattering due to abrupt refractive index changes at grain interfaces.[18] It should be noted that the interest of the research community toward luminescent materials in the form of transparent ceramics increased recently owing to the prevision of a strong lowering of manufacturing costs, especially in the field of photonics and laser technology.[19,20] Nevertheless, a primary limitation to the employment of HfO_2 powders for the latter relies in the fact that the more stable crystal polymorph at low temperature for hafnium dioxide is the monoclinic one, whereas the stability of the cubic phase occurs only at temperatures above 2500 °C.[21] This seems to preclude the possibility of overcoming the issues related to the fabrication of optical bulk materials by the ceramics method. Taking the above into consideration, the ability to control the material structure during the synthesis is a tool of major importance in the design of its optical performance and applicability. To this purpose, and considering the similarity in the chemistry of Hf and Zr, the stabilization at low temperature of the cubic polymorph of several materials including zirconia and hafnia has been already evidenced, both from theory and from experiments, through the incorporation of trivalent or even divalent ions into the lattice.[22–27] However, a majority of studies dealing with the stabilization of cubic hafnia were focused on its application as a dielectric material,[28] whereas only a few of them were guided by its potential applications in the optical field.[13,29–31] Therefore, at the present stage, there is significant room for a thorough investigation aimed at controlling the structural properties while optimizing the optical characteristics of this material.

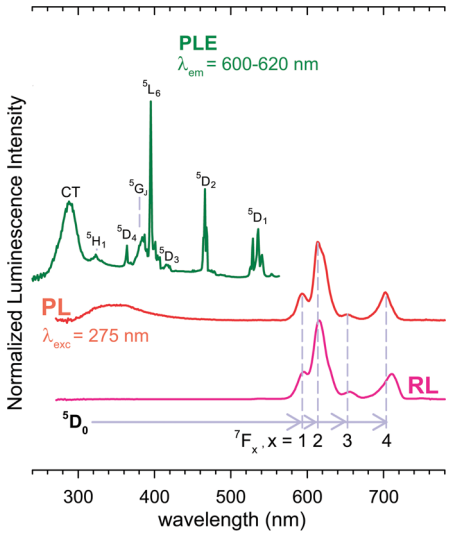

Figure 1. Room temperature PL excitation of the 600–620 nm emission range, PL emission at λ_{exc} = 275 nm and RL of HfO_2:Eu 1 mol %. The low wavelength side of the PL emission spectrum might be distorted by the presence of a long-pass filter employed to remove the excitation light.

Although the activation of luminescence in hafnia can be achieved through the incorporation of several rare earths, the presence of Eu^{3+} ions manifests optical features, which are particularly sensitive to the local crystal field.[32–35] Hence, its use as a dopant seems to be a promising tool for the fine investigation of the host crystal structure. The basic luminescence features of 1 mol % Eu^{3+} doped HfO_2 powders obtained by nonaqueous sol–gel route are summarized in Figure 1, reporting photoluminescence emission (PL) and excitation (PLE) spectra compared to its radioluminescence (RL). Both PL and RL emission spectra are dominated by the $^5D_0$–$^7F_2$ transition of Eu^{3+}, whereas the excitation spectrum of the most intense $^5D_0$–$^7F_2$ line features the transitions from $^7F_{0,1}$ levels and the charge transfer (CT) band peaking at 288 nm. Moreover, a broad composite structure below 500 nm is detected only in the PL spectrum; emissions in a similar range were already detected and attributed to optically active intrinsic defects and self-trapped excitons.[36,37] PL and RL measurements can be therefore employed in the frame of a detailed study of the synthesis parameters affecting structure and luminescence characteristics in such nanophosphors.

Among lanthanides, lutetium, when in its trivalent valence state, is not optically active due to its electronic configuration, lacking unoccupied 4f electronic levels. At the same time it is the heaviest rare earth metal, with atomic number equal to 71, immediately preceding Hf (Z = 72). Consequently, it can be expected that its incorporation might lead to the stabilization of the cubic structure with a minimum decrease of density of the material and a minimum perturbation of the emission

related to the incorporation of other activator ions. This might be advantageous especially for scintillator application demanding for an efficient absorption of ionizing radiation (X-rays, γ rays), since a high attenuation coefficient of energetic photons is related to high material density (ρ_{HfO2} = 9.6 g/cm^3) and high Z_{eff}.[21,38]

In this work, we present a facile synthesis approach where hafnium dioxide nanoparticles are obtained by non-hydrolithic sol−gel method, through a strategy where RE dopants are employed both as luminescent activators and as cubic structure stabilizers. Moreover, we exploit the strong sensitivity of 4f−4f emissions of Eu^{3+} in order to probe its site symmetry. In addition, we show that the incorporation in the lattice of optically inactive lutetium ions is effective in order to operate the structural stabilization of the cubic polymorph at room temperature. Besides the relevance in application related issues, the results here reported represent an important data set for a better comprehension of the structure−property relationship in materials confined into nanoscale dimensions.

RESULTS AND DISCUSSION

HfO_2:Eu Nanoparticles.[39] The optimization of the optical properties of nanophosphors includes, among other investigations, the identification of the optimal concentration of activator ions that gives rise to the highest luminescence efficiency. For this reason, we first investigated the structural and optical modifications operated by Eu^{3+} doping depending on its concentration.

Figure 2 shows the morphology of hafnia nanoparticles doped with different amounts of Eu^{3+}, obtained by nonaqueous sol−gel. TEM analyses allow to conclude that the synthesis leads to the formation of well dispersed nanoparticles with an elongated shape (Figure 2a−d). In accordance with previous investigations on similar reactions, due to the crystal growth mechanism where benzyl alcohol coordinates the oxide surface, agglomeration of nanoparticles is not observed.[17]

High resolution images (Figure 2b,d) show very clear lattice fringes that evidence the high crystalline grade of nanoparticles, despite its very small dimensions, irrespective of the doping level. The electron diffraction pattern recorded on the sample doped with 10 mol % Eu is compatible with the cubic structure (Figure 2e). In fact, at least the four main reflections expected from XRD are visible. This result confirms the assumption that, similarly to the case of ZrO_2, few percent trivalent ions incorporated into the lattice are able to stabilize the cubic polymorph.[22−24,40] The average linear dimension of nanoparticles has been measured to be *ca.* 3.0 ± 0.4 nm (see Table S1 in Supporting Information for size definition and determination) irrespective of the doping level, excluding a role of particle size in the achievement of the cubic polymorph stabilization (Figure 2f).

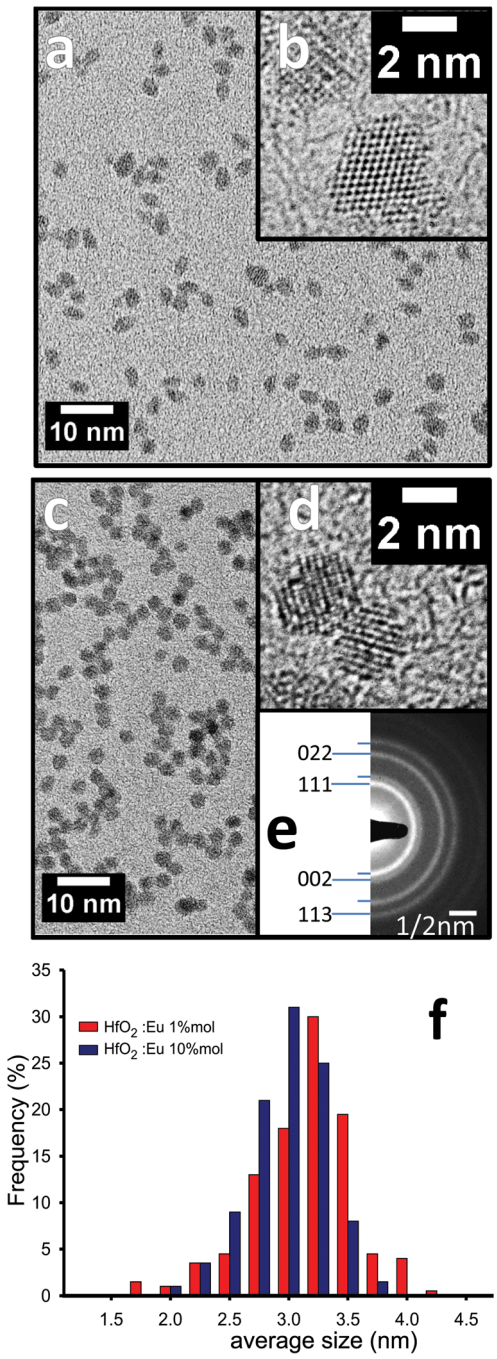

Figure 2. (a and c) TEM micrographs of HfO_2:Eu 1 mol % and HfO_2:Eu 10 mol % NPs, respectively; (b and d) HRTEM image of single particles of the same samples, respectively; (e) electron diffraction of cubic phase of HfO_2:Eu 10 mol % NPs; (f) particle size distributions of the 2 and 10 mol % Eu doped nanopowders.

A more detailed description of the structural modifications induced by doping is depicted in Figure 3. The expected monoclinic structure of hafnium dioxide is observed for Eu^{3+} concentrations up to 3 mol %, as shown by XRD (Figure 3a) according to reference ICDD PDF no. 00-006-0318. For RE concentrations exceeding 5 mol %, the diffractogram is converted to that of cubic HfO_2 as confirmed by its comparison with

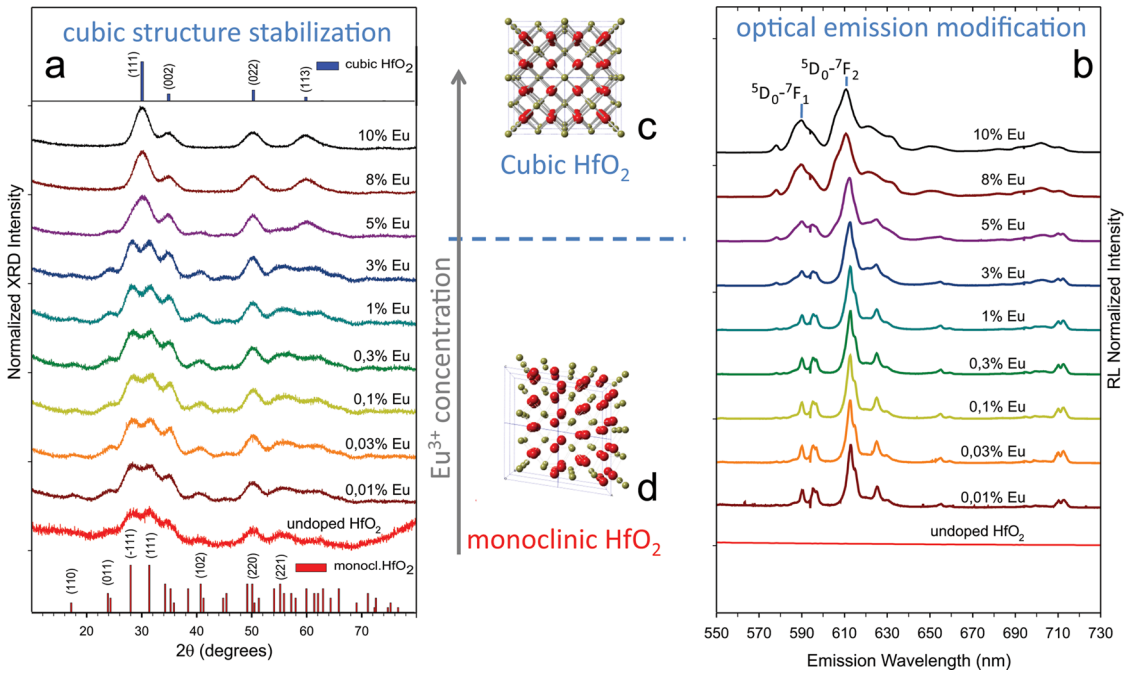

Figure 3. Structural parameters and optical emission properties of HfO_2 nanoparticles depending on the molar concentration of Eu^{3+} used as dopant. (a) XRD patterns (bar plots: calculated diffractograms from reference patterns). (b) RL spectra. For concentration of trivalent dopant higher than 5 mol %, both diffractograms and RL emissions exhibit a clear change corresponding to the stabilization of the cubic phase. (c and d) View along the *b* axis of model structure of cubic (ICSD #180833) and monoclininc (ICSD #173158) hafnia, respectively (red and yellow spheres indicate O and Hf atoms, respectively).

ICDD PDF no. 00-053-0560. Broadened diffraction peaks account for the very short range order, caused by crystalline domain sizes of just a few nanometers, confirming the TEM analyses. The actual concentration of Eu in the samples was measured by means of Induced Coupled Plasma (ICP) elemental analysis, which resulted in a value of 6.9 mol % Eu for the nominal 8 mol % sample (Table S2 in Supporting Information). As a consequence, the threshold value for the stabilization of cubic hafnia at room temperature could be set above 5 mol %. In fact, the HfO_2:Eu 5 mol % NPs exhibit a diffractogram where still 011 and 102 diffractions belonging to the monoclinic phase are present, together with major features ascribable to the cubic one, suggesting the occurrence of both structures. Considering the small volume of individual NPs, this fact could be explained by the incorporation of a sufficient number of trivalent ions inside a partial fraction of nanocrystals, while a significant portion of them is doped by Eu below the limit which is needed for a definitive structural reconfiguration. The threshold in the structure determination is also reflected by the optical emission properties, monitored by analyzing the 4f−4f transition emission in the red spectral region, stimulated by X-ray radiation (Figure 3b). The RL spectra manifest a peculiar change depending on Eu nominal concentration. Again, two families of spectra could be recognized, with an exact correlation with the crystalline structure. The same emission profile is observed in the radiative recombination of charge carriers at Eu^{3+} sites for all monoclinic hafnia nanopowders featuring a dominant $^5D_0-^7F_2$ emission line. Because this hypersensitive transition is strongly forbidden, its presence proves the lack of inversion symmetry of Eu^{3+} sites. In contrast, samples with Eu concentration higher than 5 mol % show a modified emission shape, where the relative intensities of $^5D_0-^7F_1$ and $^5D_0-^7F_2$ transitions turn out to be more similar, in accordance with the higher symmetry experienced by Eu^{3+} ions in cubic powders.[29,35] Nevertheless, the presence of the $^5D_0-^7F_2$ line and the rather large width of all optical emissions reflects the presence of different slightly distorted surroundings for Eu^{3+} incorporated inside the nanoparticles or at surface sites. These two families of correlated XRD and RL patterns confirm the role played by trivalent dopant ions in driving the crystalline structure toward the cubic symmetry.

HfO_2:Lu Nanoparticles. It can be expected that the stabilization at room temperature of the cubic polymorph of HfO_2, obtained with Eu doping above 5 mol %, could in principle be reached by employing any other rare earth with a stable trivalent or even divalent state at a similar concentration level. Nonetheless, when trying to utilize optically active lanthanides for the double purpose of either phase transformation and luminescence activation, it should be taken into account that the minimum concentration needed for the phase transformation might significantly exceed the concentration that is usually reported for the onset of detrimental luminescence quenching, that is, the concentration above which short-range non-radiative decay

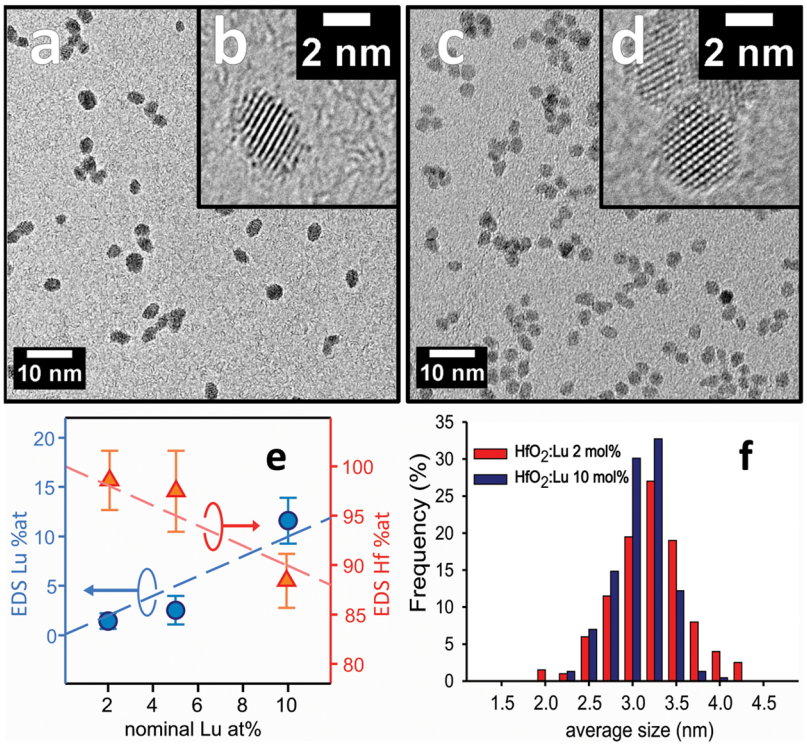

Figure 4. TEM micrographs of Lu doped HfO_2 NPs: (a) 2 mol % and (c) 10 mol % doped; insets (b and d) HRTEM of highly crystalline single particles of the same samples, respectively; (e) EDS analysis of Lu and Hf atomic concentrations depending on nominal Lu (dashed lines represent theoretical concentrations); (f) particle size distributions of the 2 and 10 mol % Lu doped hafnia nanopowders.

channels are likely to occur. Moreover, the nanophosphor luminescence could be engineered by incorporating more than one kind of dopant, in the attempt to obtain a composite emission spectrum. From this "colour tuning" perspective, it is preferable to arrange luminescent ions concentrations according exclusively to the emission spectrum required, while designating an optically inactive ion to the structural stabilization. As mentioned above, lutetium is a promising candidate for operating structural modifications with a minimal lowering of HfO_2 specific weight, and without a significant influence on the optical properties, governed by the presence of additional luminescent RE. Therefore, we synthesized Lu doped HfO_2 powders, co-doped by a minor amount of Eu^{3+}, aimed only at the activation of the luminescence and for probing the lattice geometry through its hypersensitive optical transitions.

The results of the nonaqueous synthesis of HfO_2:Lu NPs are shown in Figure 4, where morphology and composition of the products are displayed depending on concentration, ranging from 2 up to 10 mol % Lu. In a way similar to the case of HfO_2:Eu, TEM analysis reveals the formation of ultrasmall isolated NPs with a slightly elongated appearance. Energy dispersive spectroscopy (EDS) analysis (Figure 4e) shows values for final concentration of Lu in good agreement with the nominal ones. The same values are replicated also by the independent assessment by ICP elemental analysis (Table S2 in Supporting Information), confirming the performance of the method in obtaining doped nanocrystals.

The average diameter was measured to be *ca.* 3.1 ± 0.4 nm, irrespective of doping level (Figure 4f). The morphology of NPs seems to be independent of dopant concentration and type, highlighting the capability of the synthesis conditions to promote crystal growth without significant perturbations from dopants. The materials obtained indeed manifest a quite regular size distribution, irrespective of the Eu or Lu doping levels. The role played by Lu in the structural rearrangement of HfO_2 nanophospors is displayed in Figure 5, by means of the comparison between the structure, revealed by XRD measurements, and the luminescence behavior of HfO_2:Lu NPs. Data recorded on samples prepared with additional 1 mol % Eu, designed to activate luminescence, are also shown. Again, two families of materials can be obtained depending on the level of dopants inserted into the system during the synthesis procedure. More precisely, one should first consider the diffractograms measured on undoped, 2 mol % Lu, and 2 mol % Lu + 1 mol % Eu doped HfO_2 powders (Figure 5a). All these samples, containing a total level of trivalent incorporated REs of few (from 0 to 3) mol %, exhibit the same set of diffractions, comparable to that of the reference pattern of pure monoclinic hafnium dioxide (ICDD PDF no. 00-006-0318).

This fact suggests that for concentrations lower than 5 mol %, the monoclinic lattice is able to host

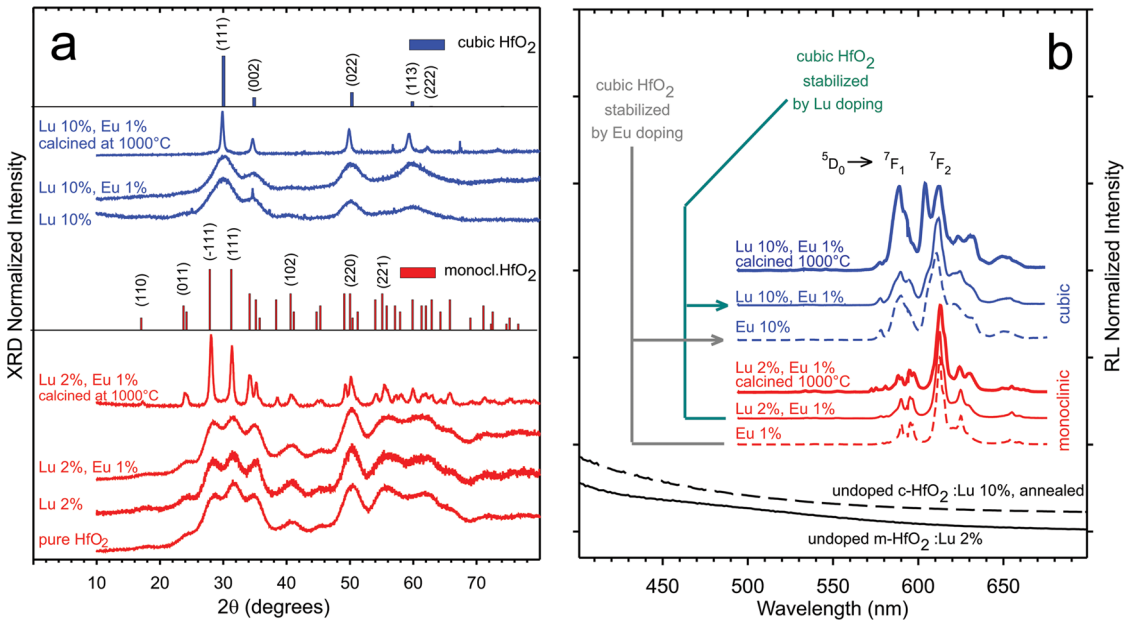

Figure 5. Structural parameters and optical emission of HfO_2 nanoparticles depending on the molar concentration of Lu^{3+} used as dopant. (a) XRD patterns (bar plots: diffractograms from reference patterns). (b) RL spectra; the introduction of Eu^{3+} ions activates the typical luminescence in the red region of the spectrum, absent in samples not containing Eu ions (black curves). The simultaneous incorporation of 2 mol % Lu^{3+} in the lattice does not affect its optical emission, which is unvaried even after calcination (red curves). Instead, 10 mol % Lu stabilizes the cubic polymorph of HfO_2, the luminescence of Eu replicates that of samples heavily doped by Eu only, and the emission modification ascribed to the luminescent site symmetry is enhanced after calcination. All curves are shifted over the ordinate axes for clarity.

the dopant without changing its geometry and the expected features belonging to the same polymorph can still be recognized. The broadening of XRD peaks accounts for the nanosized morphology of crystallites, well below 5 nm in linear length.

For a total doping exceeding 5 mol %, a structural rearrangement is observed, and the cubic polymorph features can be seen on XRD patterns of 10 mol % Lu-doped as well as of co-doped HfO_2:Lu/Eu (10, 1 mol %) NPs. Because of the broadening of peaks, it is not trivial to uniquely assign diffractions to the cubic phase of hafnia. For this reason, powder samples containing RE in a level either lower (unmodified, monoclinic) or higher (modified, cubic) with respect to the doping limit of 5 mol % were annealed in air up to 1000 °C and were examined for comparison. The results show that calcined HfO_2 nanophosphors do preserve the assigned structure on the basis of the measurements done on very small NPs. Besides the sharpening of peaks, which can be explained by the thermal promotion of crystal growth, highly doped samples exhibit the XRD peaks corresponding to single phase cubic HfO_2, as demonstrated by the now more reliable match with the reference pattern (ICDD PDF no. 00-053-0560). Figure 5b displays the optical emissions under X-ray irradiation of 4f−4f transitions of Eu^{3+} sites, used as probe for the crystal symmetry level on the same set of samples. RL spectra manifest the red luminescence corresponding to the transitions from the $^5D_0$ to ^7F_x levels of europium centers. Additionally, the spectrum modifications ascribed to the change of the activator site symmetry reflects the shift to the cubic phase, in a way quite similar to what was observed in 10 mol % Eu-doped nanoparticles. It has to be pointed out that the relative intensity change between $^5D_0$−$^7F_1$ and $^5D_0$−$^7F_2$ transitions, which reflects a higher symmetry of the Eu^{3+} site, is more evident in the calcined samples, suggesting a further lattice ordering promoted by the annealing. Such structural ordering induced by annealing is also evidenced by the more clear observation of both $^5D_0$−$^7F_1$ and $^5D_0$−$^7F_2$ split components.

These findings open to a novel design of luminescent particles where optical activators could be incorporated into host matrices with important structural transformation induced by the addition of higher amounts of an optically inactive RE, like Lu. This strategy increases the room for further applications of HfO_2 nanoscintillators, and represents a powerful tool toward a higher control of the overall functional and structural properties of innovative materials.

The easy tunability of luminescence color in structurally modified HfO_2 NPs is illustrated in Figure 6, showing RL spectra of nanopowders and photographs of their suspensions in ethanol under UV laser excitation. It is observed that the addition of Tb ions, together with Eu, gives rise to a composite luminescence spectrum featuring also the green lines at 490 and 550 nm belonging to the $^5D_4$−$^7F_{5,6}$ transitions of Tb^{3+} (well separated from Eu^{3+} emissions). As long as the total doping is only 2 mol %, the structure is unchanged and monoclinic hafnia nanophosphors are obtained. When adding also

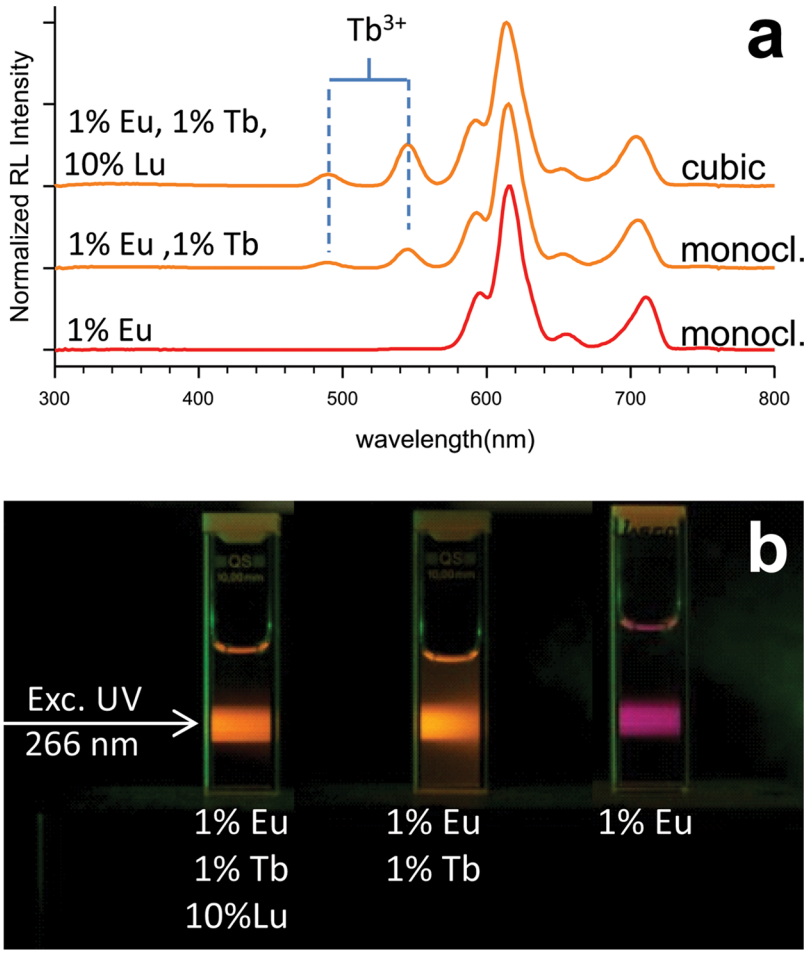

Figure 6. (a) RL of HfO_2:Eu 1 mol %, HfO_2:Eu/Tb (1, 1 mol %), and HfO_2:Lu/Eu/Tb (10, 1, 1 mol %) NPs, from bottom to top, respectively. Spectra are shifted over the ordinate axis for clarity. (b) Photograph of the same NPs suspended in ethanol, recorded under 266 nm NdYAG laser illumination.

10 mol % Lu, the structural stabilization of the polymorph is actuated and, according to XRD measurements, cubic hafnia nanophosphors are obtained. The emission profile is slightly modified, since the relative ratio between Tb^{3+} and Eu^{3+} emissions is increased in the cubic structure with respect to the monoclinic one. This suggests that the structural modification induces a crystal field change which affects (increases) more significantly the transition probabilities of Tb^{3+} emission lines.

Size Effects in Annealed Nanocrystals. Despite the promising results mentioned above, the further application of HfO_2 nanocrystals, especially as optical materials for scintillator applications, requires additional information. In fact, the extremely small size of these inorganic materials should affect its properties and represents a point of potential alteration of the optical and physical behavior. The quantum confinement and the role played by intrinsic defectiveness associated with extremely high surface area are major topics in the interpretation of data on luminescent nanocrystals.[41−43] The special nature of the synthesis mechanism here adopted, which differs strictly from many other wet and vapor-based approaches (Pechini, Sol−Gel, Atomic Layer Deposition), should be taken into account. The solvolysis of precursor molecules governed by benzyl alcohol is expected to involve the formation of organic species which could be coordinated to the surface of the inorganic nanophases. This characteristic is well documented for many metal oxides, and should be taken into account, due to its expected impact on surface chemistry and consequently on the solvent compatibility, agglomeration state and phase transformations after successive thermal treatments of the material.[44] Literature data for HfO_2 nanophosphors on this concern are not widely reported, due to the higher temperatures often involved in the synthesis procedures used for its preparation.[9,10,14,29] Therefore, a more detailed description of these materials is needed, in order to predict the evolution of its properties during further processing.

Figure 7a shows the typical TGA and DSC profile of dried as prepared NPs. A weight loss of 12% at around 450 °C associated with the main exothermal events is ascribed to the thermal decomposition of organic residuals present in the system. The vibrational spectroscopy analysis on as prepared and annealed products

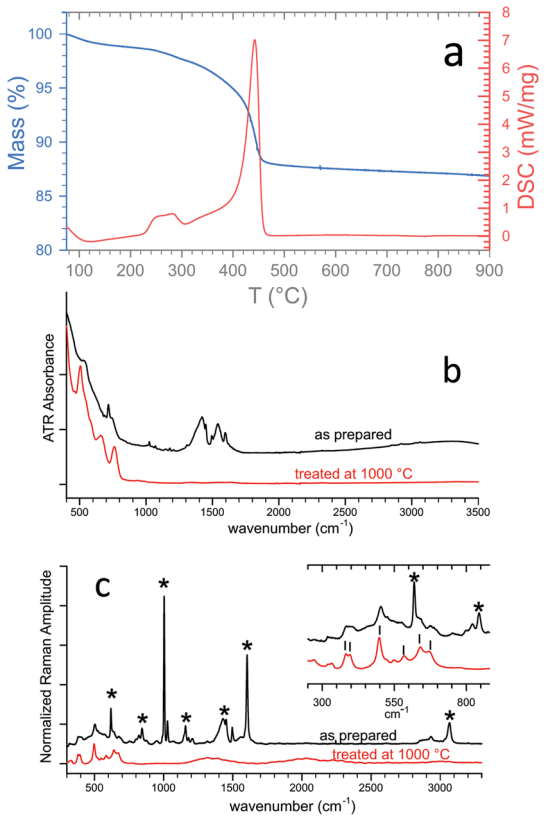

Figure 7. (a) TGA (blue line) and DSC (red line) curves of 10 mol % Lu doped HfO_2 nanopowders. (b) ATR-FTIR absorption of as prepared 2 mol % Lu (black line) and calcined 10 mol % Lu doped (red line) HfO_2 powders. (c) Raman spectra of as prepared 2 mol % Lu (black line) and calcined 10 mol % Lu doped (red line) HfO_2 powders; inset shows spectra enlarged in the low wavenumbers region (asterisks mark Raman modes of benzoate species, vertical lines mark Raman modes of HfO_2).

allowed to better identify the nature of these species. FTIR absorption measurements recorded on ATR configuration (Figure 7b) show the presence of bands at 1598, 1497, and 1450 cm^{-1} assigned to phenyl ring C═C stretch modes, while the peaks at 1545 and 1427 cm^{-1} could be ascribed to the asymmetric and symmetric stretching of COO^- groups, respectively.[45,46]

This evidence, together with the absence of OH stretching bands in the 2500−3000 cm^{-1} range, suggests the presence of benzoate groups coordinated to the nanoparticles surface, which are absent after annealing in air at 1000 °C, rather than the permanence of benzyl alcohol or benzoic acid.[47] The Raman investigation on the same materials (Figure 7c) exhibits peaks at 618, 1004, and 3066 cm^{-1} typical of phenyl rings of benzoate, together with signals at 377, 399, 495, 552, 586, 641, and 670 cm^{-1}, all ascribed to HfO_2 vibrational modes.[48−50] The comparison of these data with those of pure substances, and with data collected elsewhere on yttrium oxide nanohybrids obtained by a similar method,[51] corroborates the possible functionalization of nanoparticles by benzoate groups, decomposed as the powders are calcined above 500 °C.

Besides the removal of organic residuals, the heat treatment of the material has also a structural implication. Figure 8 describes the XRD transformation during annealing of cubic HfO_2:Lu 10 mol % NPs, and evinces the sharpening of diffraction peaks depending on temperature increase.

The average crystallite size is increased from 2.9 to 23.0 nm, according to values calculated from XRD patterns by applying the Scherrer formula on the (111) plane diffraction located at $2\theta = 30°$. Nevertheless, no peak shift is observed along the 2θ axis, suggesting that the crystalline structure does not change during this transition. HRTEM image on the same calcined sample confirms the relevant increase of crystalline domains, as well as the formation of polycrystalline larger aggregates. Also electron diffraction accounts for a limited number of crystalline orientations, associated with much larger crystallites probed by the electron beam. As expected, thermal treatments have a double effect: on one hand, the removal of organic species from the particles surfaces; on the other hand, the nanoparticles growth and their aggregation. These modifications are reflected in a change in the luminescence properties.

The measurement of the RL efficiency was employed in order to monitor the role played on the optical properties by the changes of morphology and structure associated to annealing. RL data of Eu and Eu/Lu co-doped HfO_2 are reported in Figure 9a, both before and after annealing. Untreated NPs show a monotonic increase of the RL efficiency with the Eu concentration up to 1 mol %, followed by a nearly constant signal for higher concentrations. After annealing, a considerably higher RL signal is observed at low Eu concentrations, which however does not increase significantly by varying the Eu content in the whole concentration range from 0.01 to 10 mol %. Co-doping with Lu does not seem to substantially modify the emission efficiencies.

The lack of RL increase above 1 mol % Eu for untreated samples, and in the whole concentration range for calcined samples, could suggest the presence of concentration quenching effects. For heavier dopings, it could be in fact assumed the coexistence of multiple luminescence sites in the same nanocrystal, very small before annealing. On the other hand, the calcined powders are expected to show a higher degree of compaction, a lowered average distance between luminescence sites, and the consequent quenching of the luminescence by dipole interaction even for minor Eu^{3+} dopings. However, time-resolved photoluminescence (PL) measurements of the $^5D_0-^7F_2$ transition, obtained on all annealed samples by exciting at 290 nm (see Figure S4 in Supporting Information), did not reveal any clear sign of decay acceleration or distortion depending on the doping. On the contrary, Figure 9c shows a decay time increase together with Eu concentration. Such effect could be likely related to

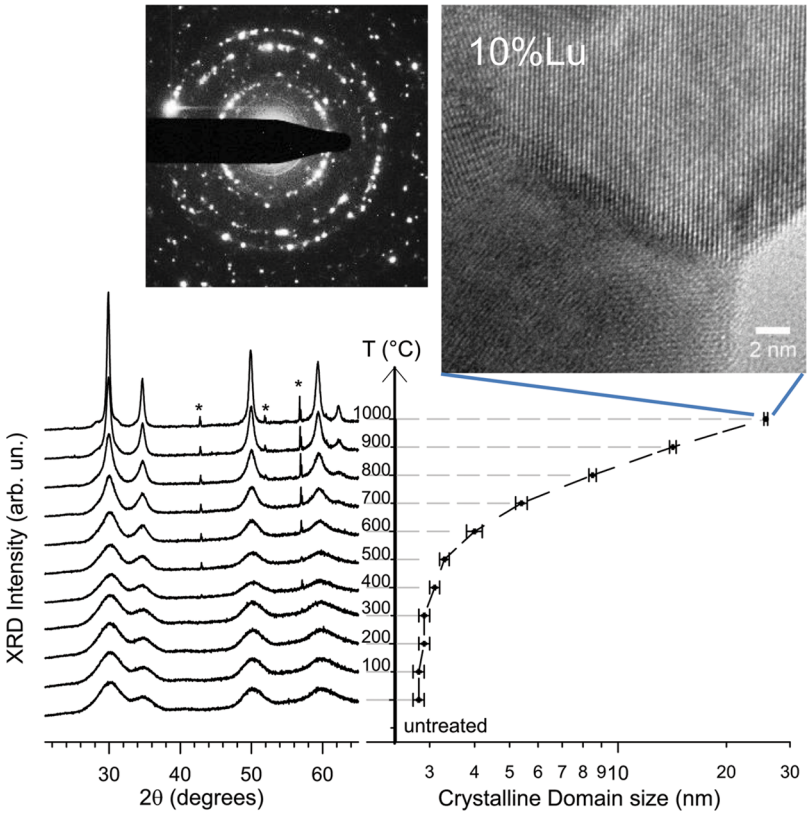

Figure 8. (Bottom left) XRD of 10 mol % Lu doped HfO_2 NPs, recorded during heating in air at successive temperatures (asterisks mark peaks arising from corundum substrate). (Bottom right) increase of crystalline domains as measured by the same diffractograms according to the Scherrer formula. (Top right) TEM micrograph of the powder treated at 1000 °C showing high crystallinity, and confirming the increase of average grain size. (Top left) electron diffraction of the same sample.

structural parameters, that is the modification from the monoclinic to the cubic lattice. The role of annealing seems that of removing non-radiative channels, which are responsible for a slight decay distortion in untreated samples, as displayed in Figure 9b for the illustrative case of the powder with 0.3 mol % Eu. Such non-radiative channels could be caused by organic residuals (absent after calcination) and surface defects (reduced by crystal growth). A decay lengthening is observed at high Eu concentrations also for untreated samples (see Figure S3 and Table S3 in Supporting Information). We note that some concentration quenching could possibly occur at concentrations higher than 1 mol %, even if no clear sign of it is revealed in time decays which are more likely governed by structural modifications.

The picture of the luminescence efficiency *versus* Eu concentration was further completed by the analysis of the intensity of steady state PL emission measurements using the same excitation and emission conditions (Figure S5 in Supporting Information). Interestingly, the comparison with RL data reveals that the PL efficiency is not significantly modified by the annealing, contrary to expectation after removal of non-radiative channels. However, the relevant error associated to these steady state measurements could prevent the clear observation of a rather weak efficiency improvement. The striking differences between PL and RL efficiencies after annealing can be explained considering the different excitation mechanisms operating in the two cases: while a selective intra-center excitation is performed for PL, free electrons and holes are the primary product of X-ray irradiation, which cause lattice ionization. Therefore, the radiative emission at Eu^{3+} centers occurs in RL only after a fast transport stage of free carriers, which migrate in the lattice losing their energy until they are captured by Eu ions. In this migration stage, carriers can also be trapped by defects which finally reduce the efficiency of radiative recombination. Therefore, it can be argued that the reduction of defect states after annealing already evidenced by the straightening of PL decays is also reflected in a much efficient carrier transfer to Eu luminescent ions occurring during the RL measurement. This explanation however does not justify the lack of signal increase observed in annealed samples when the Eu concentration increases. This finding deserves further investigations and only hypothetical explanations can be here proposed; for example, it could be supposed that trivalent Eu incorporated in high concentrations in HfO_2 can be the cause of additional, rare-earth driven point defects causing self-absorption of the emitted light.

Finally, the PLE and PL data of HfO_2:Lu/Eu (10, 1 mol %) powder are reported in Figure 10. The excitation spectrum of the $^5D_0 - ^7F_2$ transition at 612 nm shows the charge transfer (CT) band peaking at 285 and 293 nm before and

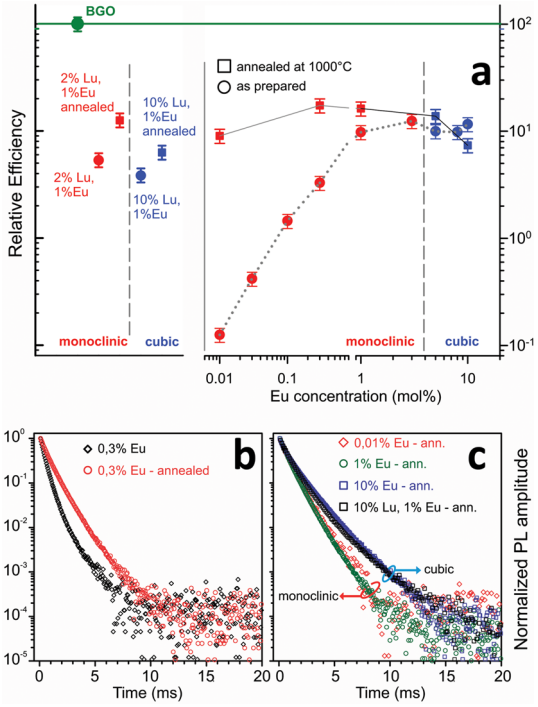

Figure 9. (a, left) RL efficiencies of hafnia nanoparticles co-doped with Lu (2 and 10 mol %) and Eu (1 mol %), before and after heat treatment at 1000 °C (BGO refers to Bismuth Germanate powder shown as reference). (a, right) RL efficiencies of as prepared (dotted line) and treated (full line) Eu doped HfO_2 NPs, depending on nominal Eu concentration (values determined as integrals over the 500−750 nm range of RL spectra recorded in the same conditions). (b) Room temperature PL decays of 0.3 mol % Eu doped HfO_2 nanoparticles before and after annealing at 1000 °C. λ_{exc} = 290 nm, λ_{em} = 613 nm. (c) Room temperature PL decays of Eu doped HfO_2 nanoparticles after annealing at 1000 °C. λ_{exc} = 290 nm, λ_{em} = 613 nm.

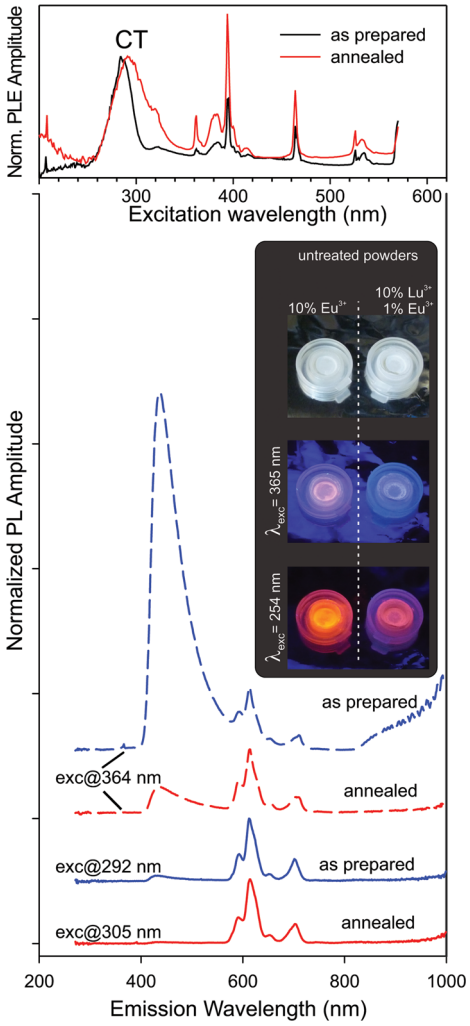

Figure 10. (Top panel) PL excitation (PLE) spectra of the 600−620 nm emission range of HfO_2: Lu/Eu (10, 1 mol %) before (black line) and after (red line) treatment at 1000 °C (spectra normalized to CT maximum). (Bottom panel) PL emission (PL) spectra of HfO_2:Lu/Eu (10, 1 mol %) before (blue lines) and after (red lines) annealing, with λ_{exc} = 364 nm (dashed lines) and in CT (full lines) at λ_{exc} = 292 or 305 nm (all emission spectra normalized at 612 nm, and shifted over the ordinate axis for clarity; spectra are altered in the higher energy region by the use of a cutoff filter at 418 nm). Inset: optical images taken on untreated powders by exciting with the 365 or 254 nm lines of a Wood's lamp.

after the thermal treatment, respectively, whereas the Eu^{3+} transitions from $^7F_{0,1}$ levels are significantly increased by calcination (Figure 10, top panel). The PL emission spectrum of the untreated sample excited at 364 nm is dominated by a broad blue band, which vanishes by exciting at 292 nm where, in turn, only Eu^{3+} red emission is detected (Figure 10, bottom panel). After the thermal treatment, the PL emission spectra are dominated by the forbidden $^5D_0-^7F_2$ transition of Eu^{3+}: a broad luminescence band covering the high energy side of the spectrum is observed exciting at 364 nm.

Hence, the material exhibits an evident spectral emission modification by slightly changing the excitation wavelength, also depending on thermal treatment. The inset in Figure 10 shows photographs of cubic phase HfO_2 NPs (Eu 10 mol % and Lu/Eu (10, 1 mol %), respectively) illuminated with the two lines of a common Wood's lamp. Here, the 365 nm line well excites the blue emission and only partially excites the Eu-related red emission. As a consequence, the excitation with the lower energy line results in a pink emission for the higher concentration of europium, whereas the blue component dominates in the sample with only 1 mol % Eu.

CONCLUSIONS

A synthesis strategy disclosing the multifunctional role of RE doping in luminescent HfO_2 nanoscintillators obtained through the nonaqueous sol−gel method was presented. The detailed study of the structural modifications induced by the incorporation of trivalent RE reveals that a concentration of at least 5 mol % is needed in order to stabilize the cubic polymorph of hafnia nanoparticles at room temperature. The results demonstrate the possibility to induce luminescent properties through the doping

with one or more RE activators, while the structural stabilization can be simultaneously carried out by co-doping with nonluminescent Lu^{3+} ions, in higher amounts. These findings open the way for a high level of control on the functional/structural properties through the appropriate choice of dopants and their concentrations in a one-pot synthesis procedure. Moreover, in the perspective of its application as optical nanocomposites or ceramics, the transformations occurring during thermal treatments helped to predict both the stability of the modified crystalline cubic phases and the optical performance gain. Finally, it was possible to highlight a luminescence color switch depending on excitation wavelength thanks to the selective excitation of intrinsic or activator-related emissions.

EXPERIMENTAL SECTION

Materials. Hafnium(IV) *tert*-butoxide (99.99%+ Zr) and lutetium acetate hydrated were purchased from Multivalent Laboratory, Eriswell, U.K. Europium(III) acetate hydrate (99.99%), terbium(III) acetate hydrate (99.9%), and benzyl alcohol anhydrous (99.8%) were purchased from Sigma-Aldrich. All precursors were used as received.

Synthesis of HfO_2 Nanoparticles. Syntheses by nonaqueous sol–gel were carried out in a glovebox (O_2 and H_2O < 0.1 ppm). In a typical synthesis, hafnium(IV) *t*-butoxide was added to anhydrous benzyl alcohol (BnOH) into a glass test tube. For doped samples, the appropriate volumes of the acetates predissolved in BnOH were mixed to the solvent before addition of Hf precursor. A total amount of 2.4 mmol of precursor and a total volume of 20 mL mixtures were used. The reaction mixture was transferred into a Teflon liner of 45 mL, slid into a steel autoclave (acid digestion vessel mod. 4744 by Parr Instrument Company) and carefully sealed. The autoclave was taken out of the glovebox and heated in a furnace at 220 °C for 96 h. The synthesis resulted on a milky suspension that was centrifuged; the precipitate was thoroughly washed with diethyl ether (Aldrich) and then dried in air at 60 °C overnight.

Characterization. All X-ray diffraction (XRD) measurements were performed in reflection mode (Cu Ka radiation at 45 kV and 40 mA) either on a XPertPro diffractometer or on an Empyrean diffractometer (equipped with a high temperature chamber model HTK 1200 from Anton Paar), both from PANalytical (The Netherlands).

Differential scanning calorimetry and thermogravimetry (TG/DSC) were performed on a Netsch STA 449C; samples were prepared by placing nanopowders in Pt crucibles with a lid, and measured in Ar/O_2 flux against empty Pt crucibles as a reference. A subsequent cycle was performed on the annealed sample as correction measurement.

Energy Dispersive X-ray Spectroscopy (EDS) measurements were measured on a Zeiss Leo Gemini 1530. Induced Coupled Plasma (ICP) elemental analysis was achieved through a Perkin-Elmer ICP-OES Optima 7000 DV.

TEM measurements were made on a Philips FEI Tecnai F30 microscope operated at 300 kV on samples prepared by depositing onto carbon coated Cu grids 10 μL of ethanol (Aldrich) suspension of washed NPs.

Attenuated total reflectance (ATR) measurements were performed on a Bruker Alpha FT-IR Spectrometer equipped with diamond ATR optics. MicroRaman spectra were collected in backscattering configuration using the 633 nm line of a He–Ne laser on a Labram Dilor spectrometer.

The radioluminescence (RL) measurements were carried out at room temperature (RT) using a homemade apparatus featuring, as detection system, a charge coupled device (CCD) (Jobin-Yvon Spectrum One 3000) coupled to a spectrograph operating in the 200–1100 nm range (Jobin-Yvon Triax 180). The data were corrected for the spectral response of the detection system. RL excitation was obtained by X-rays irradiation through a Be window, using a Philips 2274 X-ray tube with tungsten target operated at 20 kV. The data were corrected for the spectral response of the detection system.

Time-resolved photoluminescence (PL) measurements were performed at RT by a Varian Eclipse spectrofluorimeter. Steady state PL spectra were measured at RT by a xenon lamp as excitation source, together with a double monochromator (Jobin-Yvon Gemini 180 with a 1200 grooves/mm grating), and recorded through a nitrogen cooled CCD detector coupled to a monochromator (Jobin-Yvon Micro HR).

Conflict of Interest: The authors declare no competing financial interest.

Supporting Information Available: TEM statistical analysis and micrograph of calcined NPs, ICP-OE elemental analysis, Raman comparison of HfO_2 (both cubic and monoclinic) and Lu_2O_3, time-resolved PL measurements and analysis. This material is available free of charge *via* the Internet at http://pubs.acs.org.

Acknowledgment. The authors would like to acknowledge C. Canevali from University of Milano–Bicocca for Induced Coupled Plasma (ICP) elemental analysis and M. J. Süess from EMEZ for Transmission Electron Microscopy (TEM) imaging. R. Lorenzi of University of Milano–Bicocca is gratefully acknowledged for digital imaging under UV laser illumination. We gratefully acknowledge the financial support of ETH Zurich and of the Italian CARIPLO Foundation project "Energy transfer and trapping processes in nanostructured scintillator materials" (2008–2011).

REFERENCES AND NOTES

1. Robertson, J. High Dielectric Constant Gate Oxides for Metal Oxide Si Transistors. *Rep. Prog. Phys.* **2006**, *69*, 327–396.
2. Wilk, G. D.; Wallace, R. M.; Anthony, J. M. High-Kappa Gate Dielectrics: Current Status and Materials Properties Considerations. *J. Appl. Phys.* **2001**, *89*, 5243–5275.
3. Fujimori, H.; Yashima, M.; Sasaki, S.; Kakihana, M.; Mori, T.; Tanaka, M.; Yoshimura, M. Internal Distortion in Ceria-Doped Hafnia Solid Solutions: High-Resolution X-Ray Diffraction and Raman Scattering. *Phys. Rev. B: Condens. Matter Mater. Phys.* **2001**, *64*, 134104.
4. Wang, J.; Li, H. P.; Stevens, R. Hafnia and Hafnia-Toughened Ceramics. *J. Mater. Sci.* **1992**, *27*, 5397–5430.
5. Crepeau, J. C.; Rempe, J. L.; Daw, J. E.; Knudson, D. L.; Condie, K. G.; Wilkins, S. C. *Enhancements to High Temperature in-Pile Thermocouple Performance*; DOE/ID/14738, INL/EXT-08-14042; TRN: US200816%%891; National Technical Information Center: Oak Ridge TN, **2008**.
6. Cheynet, M. C.; Pokrant, S.; Tichelaar, F. D.; Rouviere, J. L. Crystal Structure and Band Gap Determination of HfO_2 Thin Films. *J. Appl. Phys.* **2007**, *101*.
7. Lange, S.; Kiisk, V.; Aarik, J.; Kirm, M.; Sildos, I. Luminescence of ZrO_2 and HfO_2 Thin Films Implanted with Eu and Er Ions. *Phys. Status Solidi C* **2007**, *4*, 938–941.
8. Lange, S.; Kiisk, V.; Reedo, V.; Kirm, M.; Aarik, J.; Sildos, I. Luminescence of RE-Ions in HfO_2 Thin Films and Some Possible Applications. *Opt. Mater.* **2006**, *28*, 1238–1242.
9. LeLuyer, C.; Villanueva-Ibañez, M.; Pillonnet, A.; Dujardin, C. HfO_2:X (X = Eu^{3+}, Ce^{3+}, Y^{3+}) Sol Gel Powders for Ultradense Scintillating Materials. *J. Phys. Chem. A* **2008**, *112*, 10152–10155.
10. Meng, J.; Jiang, D.; Li, Q. Luminescent Properties of Eu^{3+}-Doped HfO_2 Powders Prepared by Combustion. *Key Eng. Mater.* **2010**, *434–435*, 805–807.

11. Wiatrowska, A.; Zych, E. Modeling Luminescent Properties of HfO_2:Eu Powders with Li, Ta, Nb, and V Codopants. *J. Phys. Chem. C* **2012**, *116*, 6409–6419.
12. Cushing, B. L.; Kolesnichenko, V. L.; O'Connor, C. J. Recent Advances in the Liquid-Phase Syntheses of Inorganic Nanoparticles. *Chem. Rev.* **2004**, *104*, 3893–3946.
13. Taniguchi, T.; Sakamoto, N.; Watanabe, T.; Matsushita, N.; Yoshimura, M. Rational Hydrothermal Route to Monodisperse $Hf_{1-x}Eu_xO_{2-x/2}$ Solid Solution Nanocrystals. *J. Phys. Chem. C* **2008**, *112*, 4884–4891.
14. Wiatrowska, A.; Zych, E.; Kępiński, L. Monoclinic HfO_2:Eu X-Ray Phosphor. *Radiat. Meas.* **2010**, *45*, 493–496.
15. Buha, J.; Arcon, D.; Niederberger, M.; Djerdj, I. Solvothermal and Surfactant-Free Synthesis of Crystalline Nb_2O_5, Ta_2O_5, HfO_2, and co-Doped HfO_2 Nanoparticles. *Phys. Chem. Chem. Phys.* **2010**, *12*, 15537–15543.
16. Pinna, N.; Garnweitner, G.; Antonietti, M.; Niederberger, M. Non-Aqueous Synthesis of High-Purity Metal Oxide Nanopowders Using an Ether Elimination Process. *Adv. Mater.* **2004**, *16*, 2196–2200.
17. Pinna, N.; Niederberger, M. Surfactant-Free Nonaqueous Synthesis of Metal Oxide Nanostructures. *Angew. Chem., Int. Ed.* **2008**, *47*, 5292–5304.
18. Krell, A.; Hutzler, T.; Klimke, J. Transmission Physics and Consequences for Materials Selection, Manufacturing, and Applications. *J. Eur. Ceram. Soc.* **2009**, *29*, 207–221.
19. Ikesue, A.; Aung, Y. L. Ceramic Laser Materials. *Nat. Photonics* **2008**, *2*, 721–727.
20. Shi, Y.; Nikl, M.; Feng, X.; Mares, J. A.; Shen, Y.; Beitlerova, A.; Kucerkova, R.; Pan, Y.; Liu, Q. Microstructure, Optical, and Scintillation Characteristics of Pr^{3+} Doped $Lu_3Al_5O_{12}$ Optical Ceramics. *J. Appl. Phys.* **2011**, *109*, 013522–7.
21. Cardarelli, F. *Material Handbook: A Concise Desktop References*, 2nd ed.; Springer Verlag: New York, 2008.
22. Lu, C.-H.; Raitano, J. M.; Khalid, S.; Zhang, L.; Chan, S.-W. Cubic Phase Stabilization in Nanoparticles of Hafnia-Zirconia Oxides: Particle-Size and Annealing Environment Effects. *J. Appl. Phys.* **2008**, *103*, 124303–7.
23. Ghosh, A.; Suri, A. K.; Pandey, M.; Thomas, S.; Rama Mohan, T. R.; Rao, B. T. Nanocrystalline Zirconia-Yttria System – a Raman Study. *Mater. Lett.* **2006**, *60*, 1170–1173.
24. Bhagwat, M.; Ramaswamy, A. V.; Tyagi, A. K.; Ramaswamy, V. Rietveld Refinement Study of Nanocrystalline Copper Doped Zirconia. *Mater. Res. Bull.* **2003**, *38*, 1713–1724.
25. Jiang, C.; Wang, F.; Wu, N.; Liu, X. Up- and Down-Conversion Cubic Zirconia and Hafnia Nanobelts. *Adv. Mater.* **2008**, *20*, 4826–4829.
26. Wang, F.; Han, Y.; Lim, C. S.; Lu, Y.; Wang, J.; Xu, J.; Chen, H.; Zhang, C.; Hong, M.; Liu, X. Simultaneous Phase and Size Control of Upconversion Nanocrystals through Lanthanide Doping. *Nature* **2010**, *463*, 1061–1065.
27. Teng, X.; Zhu, Y.; Wei, W.; Wang, S.; Huang, J.; Naccache, R.; Hu, W.; Tok, A. I. Y.; Han, Y.; Zhang, Q.; *et al.* Lanthanide-Doped Na_xScF_{3+X} Nanocrystals: Crystal Structure Evolution and Multicolor Tuning. *J. Am. Chem. Soc.* **2012**, *134*, 8340–8343.
28. Dubourdieu, C.; Rauwel, E.; Roussel, H.; Ducroquet, F.; Hollander, B.; Rossell, M.; Van Tendeloo, G.; Lhostis, S.; Rushworth, S. Addition of Yttrium into HfO_2 Films: Microstructure and Electrical Properties. *J. Vac. Sci. Technol., A* **2009**, *27*, 503–514.
29. Zych, E.; Wójtowicz, M.; Dobrowolska, A.; Kępiński, L. Radioluminescence and Photoluminescence of Hafnia-Based Eu-Doped Phosphors. *Opt. Mater.* **2009**, *31*, 1764–1767.
30. Wang, Y. J.; Wu, T.; Kanamori, Y.; Hane, K. Freestanding HfO_2 Grating Fabricated by Fast Atom Beam Etching. *Nanoscale Res. Lett.* [Online] **2011**, *6*, 367. http://www.nanoscalereslett.com/content/6/1/367.
31. Nedelec, J. M. Sol-Gel Processing of Nanostructured Inorganic Scintillating Materials. *J. Nanomater.* [Online] **2007**, *2007*, No. Article ID 36392. DOI:10.1155/2007/36392.
32. Francini, R. Spectroscopy of Rare-Earth Ions in Insulating Materials. *Proc. SPIE* **1997**, *3176*, 2–11.
33. Reisfeld, R. Spectroscopy of Rare Earth Ions. In *Nanostructured and Advanced Materials for Applications in Sensor, Optoelectronic and Photovoltaic Technology*; Vaseashta, A., Dimova-Malinovska, D., Marshall, J. M., Eds.; Springer: The Netherlands, 2005; Vol. 204, pp 77−100.
34. Binnesmans, K.; Gorller-Warland, C. Application of the Eu^{3+} Ion for Site Symmetry Determination. *J. Rare Earths* **1996**, *14*, 173–180.
35. Zych, E. Concentration Dependence of Energy Transfer between Eu^{3+} Ions Occupying Two Symmetry Sites in Lu_2O_3. *J. Phys.: Condens. Matter* **2002**, *14*, 5637.
36. Chuang, S.-H.; Lin, H.-C.; Chen, C.-H. Oxygen Vacancy Relationship to Photoluminescence and Heat Treatment Methods in Hafnium Oxide Powders. *J. Alloys Compd.* **2012**, *534*, 42–46.
37. Kiisk, V.; Lange, S.; Utt, K.; Tatte, T.; Mandar, H.; Sildos, I. Photoluminescence of Sol-Gel-Prepared Hafnia. *Phys. B* **2010**, *405*, 758–762.
38. Rodnyi, P. A. *Physical Processes in Inorganic Scintillators*; CRC Press LLC; Boca Raton, FL, 1997.
39. In this work we refer to hafnia nanocrystals doped with rare earths ions as follows: HfO_2:RE *x* mol % (RE = Lu, Eu; *x* = nominal concentration in the initial solutions). Samples doped with more than one element are named as HfO_2: $RE_1/RE_2/RE_3$ (c1, c2, c3 mol %). All samples are mentioned according to the nominal concentration (c1, c2, c3) in the initial solutions.
40. Li, P.; Chen, I. W.; Penner-Hahn, J. E. Effect of Dopants on Zirconia Stabilization—An X-Ray Absorption Study: I, Trivalent Dopants. *J. Am. Ceram. Soc.* **1994**, *77*, 118–128.
41. Rauwel, P.; Rauwel, E.; Persson, C.; Sunding, M. F.; Galeckas, A. One Step Synthesis of Pure Cubic and Monoclinic HfO_2 Nanoparticles: Correlating the Structure to the Electronic Properties of the Two Polymorphs. *J. Appl. Phys.* **2012**, *112*, 104107–8.
42. Mercier, B.; Ledoux, G.; Dujardin, C.; Nicolas, D.; Masenelli, B.; Melinon, P.; Bergeret, G. Quantum Confinement Effect on Gd_2O_3 Clusters. *J. Chem. Phys.* **2007**, *126*, 044507–7.
43. LeBihan, V.; Pillonnet, A.; Amans, D.; Ledoux, G.; Marty, O.; Dujardin, C. Critical Dimension Where the Macroscopic Definition of Refractive Index Can Be Applied at a Nanometric Scale. *Phys. Rev. B: Condens. Matter Mater. Phys.* **2008**, *78*, 113405.
44. Niederberger, M.; Pinna, N. *Metal Oxide Nanoparticles in Organic Solvents*; Springer Verlag: London, 2009.
45. Dobson, K. D.; McQuillan, A. J. *In Situ* Infrared Spectroscopic Analysis of the Adsorption of Aromatic Carboxylic Acids to TiO_2, ZrO_2, Al_2O_3, and Ta_2O_5 from Aqueous Solutions. *Spectrochim. Acta, Part A* **2000**, *56*, 557–565.
46. Koutstaal, C. A.; Ponec, V. FT-IR Study on the Adsorption of Benzoic Acid and its Derivatives on Transition-Metal Oxides. *Appl. Surf. Sci.* **1993**, *70−71* (Part 1), 206–210.
47. Bai, X.; Pucci, A.; Freitas, V. T.; Ferreira, R. A. S.; Pinna, N. One-Step Synthesis and Optical Properties of Benzoate- and Biphenolate-Capped ZrO_2 Nanoparticles. *Adv. Funct. Mater.* **2012**, *22*, 4275–4283.
48. Kim, B.-K.; Hamaguchi, H.-o. Raman Spectrum of ^{18}O-Labelled Hafnia. *Mater. Res. Bull.* **1997**, *32*, 1367–1370.
49. Quintard, P. E.; Barberis, P.; Mirgorodsky, A. P.; Merle-Mejean, T. Comparative Lattice-Dynamical Study of the Raman Spectra of Monoclinic and Tetragonal Phases of Zirconia and Hafnia. *J. Am. Ceram. Soc.* **2002**, *85*, 1745–1749.
50. Fujimori, H.; Yashima, M.; Sasaki, S.; Kakihana, M.; Mori, T.; Tanaka, M.; Yoshimura, M. Cubic-Tetragonal Phase Change of Yttria-Doped Hafnia Solid Solution: High-Resolution X-Ray Diffraction and Raman Scattering. *Chem. Phys. Lett.* **2001**, *346*, 217–223.
51. Pinna, N.; Garnweitner, G.; Beato, P.; Niederberger, M.; Antonietti, M. Synthesis of Yttria-Based Crystattine and Lamellar Nanostructures and Their Formation Mechanism. *Small* **2005**, *1*, 112–121.